The seasonal cycle in the Atlantic transport to the Barents Sea during the years 1997–2001

R.B.Randi B. Ingvaldsen, Lars Asplin and Harald Loeng

Institute of Marine Research, P.O. Box 1870, Nordnes, N-5024, Bergen, Norway

Abstract

The seasonal cycle in the Atlantic inflow to the Barents Sea is investigated by using 4-year long records from moored current meters, additional moorings of shorter duration, and hydrographic measurements. A higher transport during winter than summer is most common, but in years where the Barents Sea climate changes from a climatically cold to a climatically warm period (and probably vice versa), it may differ substantially from this. The higher transport during winter is related to barotropic currents that are forced by sea-level changes within the section induced by a shear in the cross-section wind stress, although possibly enhanced by variations in the remotely forced Norwegian Atlantic Current. The seasonal variation within the section is not uniform, and the strongest seasonal signal is found in the middle and northern parts. In the area near 71°30′N the wind (both speed and direction) changes substantially from winter to summer, without changes of the net Ekman transport. The water-level gradient, and the associated barotropic current, therefore has no seasonal variation in this area. However, there is a seasonal signal in the front between the Atlantic and Coastal Waters near the Norwegian Coast. This is due to coastal downwelling during winter that is forced by strong southwesterly winds. The mean transport of Atlantic Water is estimated to 1.7 Sv (1 Sv=10^6 m^3 s^{-1}) during winter and 1.3 Sv during summer, but there is a pronounced minimum in Atlantic inflow (or even outflow) in spring due to an annual event of northerly winds.

Author Keywords: Volume transport; Seasonal cycle; Barotropic motion; Ekman transport; Nordic Seas; Barents Sea; Barents Sea Opening

1. Introduction

The inflow of Atlantic Water (AW) is of crucial importance for the physical and ecological conditions of the Barents Sea. With the inflowing AW, fish larvae and zooplankton are advected into the Barents Sea from the Norwegian Sea (e.g. Ozhigin and Ushakov, 1985; Skjoldal and Rey, 1989; Skjoldal et al., 1992;

Giske et al., 1998). The climatic conditions affect the growth rate and distribution of zooplankton and fish larvae, as well as fish population parameters as growth, recruitment, migration and distribution (e.g. Ottersen and Loeng, 2000; Stenseth et al., 2002). Recent publications have proposed that a warming of the Barents Sea may lead to a redistribution of the commercial important fish species in the Barents Sea (Blindheim et al., 2001). Thus, an understanding of the variability of the Atlantic inflow is highly important.

The Barents Sea also influences the Arctic Ocean; not only by providing a pathway for AW to the Arctic Ocean, but also as a shallow shelf sea producing dense water through cooling and brine release. When passing through the Barents Sea the AW is strongly modified by cooling, mixing and freezing during winter, and all the AW entering in the west is modified and leaves the shelf toward the Arctic Ocean mostly with temperatures below 0°C (Schauer et al., 2002b). According to Schauer et al. (2002a), the Barents Sea plays a special role among the other shelf seas considering the ventilation of the Arctic Ocean because: (1) being close to the Norwegian Sea it receives the most saline marine inflow, (2) through its permanent inflow from the Nordic Seas it continuously supplies water to the central Arctic basins (Rudels, 1987; Rudels et al., 1994), (3) being the deepest Arctic shelf sea, and (4) by receiving only little river input. Observations have shown that the Barents Sea provide intermediate water down to 1200 m depth in the Arctic Ocean (Rudels et al., 1994; Schauer et al., 1997), and, together with the Kara Sea, the Barents Sea is the only source area for shelf waters ventilating the Nansen Basin below the halocline (Schauer et al., 1997). Recent investigations suggest that the throughflow of AW also can take part in a process where water distilled at the surface of the Arctic by freezing ends up at mid-depth in the same ocean (Aagaard and Woodgate, 2001). The process starts with an increase in the export of ice from the Arctic Ocean into the Barents Sea. The ice melts due to contact with the AW; whereby the melt water is entrained in the Barents Sea throughflow and subsequently sinks into the Arctic Ocean (Aagaard and Woodgate, 2001). Woodgate et al. (2001) ascribed an observed cooling and freshening of the Atlantic layer in the Arctic to this process, and also Schauer et al. (2002b) pointed out that the observed freshening was due to a larger input of fresh water to the Barents Sea. Thus, knowledge of the variability of the Atlantic inflow to the Barents Sea, and quantification of the volume transports, is important for the understanding of the climatic state of a wider region, and for evaluations of climate change.

The main inflow of AW to the Barents Sea takes place in the Norwegian Atlantic Current (NAC) through the Barents Sea Opening (BSO) (Fig. 1). Along the Norwegian Coast, the Norwegian Coastal Current (NCC) brings relatively fresh and warm water into the Barents Sea. During winter, the NCC is deep and narrow, while during summer it is wide and shallow (Sætre and Ljøen, 1971). North of the NAC, the Bear Island Current takes relatively colder and fresher water of Arctic origin out of the Barents Sea.

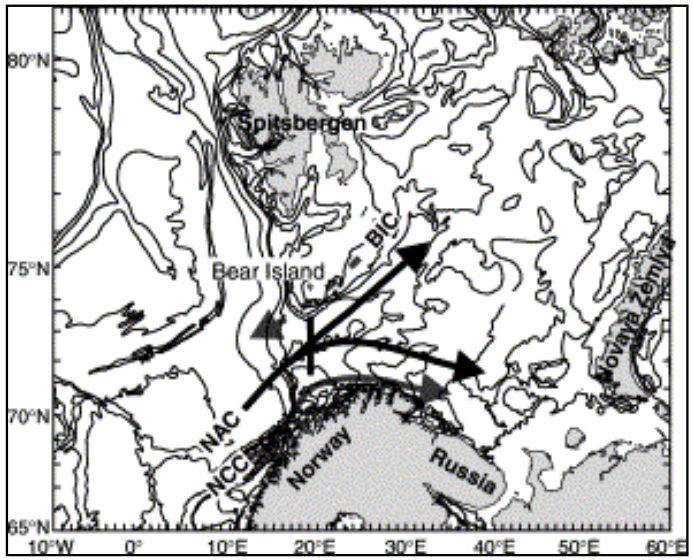

Fig. 1. Map of the Barents Sea and the main current systems. NAC: the Norwegian Atlantic Current, NCC: the Norwegian Coastal Current, and BIC: the Bear Island Current. The solid line shows the section where the current meter moorings were deployed.

Several previous studies have given estimates of the volume flux across the BSO, but moored current measurements in the area have been rare. Prior to our measurements the only transports based on moored current meters were from a 2-month time series (Blindheim, 1989). All other published estimations of volume fluxes have been based on vessel-mounted Acoustic Doppler Profiler (Haugan, 1999; O'Dwyer et al., 2001), as well as budget considerations (Loeng et al., 1997; Haugan, 1999), numerical modelling (e.g. Parsons, 1995), and geostrophic calculations of the baroclinic currents (numerous Russian studies). A seasonal cycle with a higher inflow during winter than summer has been inferred based on the general wind field (Ådlandsvik and Loeng, 1991; Harms, 1992; Furevik, 1998), on investigations upstream in the Norwegian Sea (Orvik et al., 2001), on the geostrophic calculations, and on current measurements in the eastern Barents Sea (Loeng et al., 1993). However, the physical explanation to the deduced seasonality was not identified.

In this paper, we use the 4-year long time series from an array of moored current meters in the main Atlantic inflow in the BSO (Fig. 2). We also consider two additional moorings on the slope south of Bear Island, hydrographic sections, 10-m wind field, and sea-level height as obtained from a numerical model. The investigation addresses the seasonal variation in the Atlantic inflow during the period 1997–2001, and emphasizes these issues: (1) description and quantification of the exchanges of AW between the Norwegian and the Barents Seas, and (2) identification of the forcing responsible for the variations in the Atlantic inflow. The focus on the AW may seem unfortunate. The inflow of Coastal Water in the NCC is 0.5–1 Sv, 30–75% of the AW transport, and has a large impact on the transformation of the AW in the Barents Sea. The amount of outflow of cold, less saline Arctic Water in the Bear Island Current is unknown, but clearly important for the volume, heat and salt balances of the Arctic Ocean. The seasonal variability in both these currents may be as interesting as the seasonal changes in the flow of AW. The limitation to the AW is due to the extension of the mooring array, which does not give sufficient coverage in the southern and northern parts of the passage. Additional moorings will be deployed in the NCC and the Bear Island Current in September 2003, and the variability in these currents will be a supplement to this investigation.

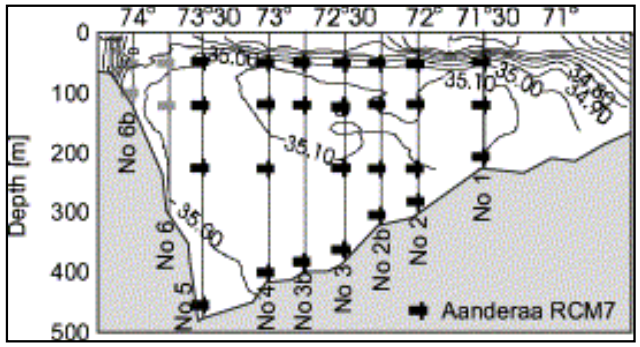

Fig. 2. Salinity in August 1998 and location of all the moorings and instruments. Black boxes denote instruments included in the 4-year time series, grey boxes instruments from the short time moorings. Information of the moorings and instruments in the 4-year time series are given in Table 1.

The paper is organized as follows: In Section 2, the data are presented, while Section 3 deals with description and quantification of the AW transport. In Section 4, the results presented in Section 3 are discussed and the forcing responsible for the seasonal variations is investigated. The results are summarized and concluded in Section 5. The 4-year time series from the moored current meters is the same as used by Ingvaldsen et al. (2004), but then with the focus on giving a description of the observed velocity field.

2. Description of the data

The 4-year records consist of velocity and temperature measurements from moored Aanderaa Recording Current Meter 7 (RCM7) deployed between 71°30′N and 73°30′N in the period from August 1997 to August 2001 (Fig. 2 and Table 1). The number of moorings deployed, and the number of instruments attached to each mooring, varied over the period. Data were recorded every 20 min, but were sub-sampled to daily values for this analysis. To fill gaps in the time series due to missing single instruments (Table 1, lower panel), simple linear interpolation of the velocities from the instrument above and/or below was performed. This is an adequate method since the velocities are mostly barotropic (e.g. Blindheim, 1989). When moorings No. 2b and 3b were not deployed, interpolated values from the two surrounding moorings were used. For the period January–August 1999 mooring No. 1 was missing, and the values from mooring No. 2 were extrapolated to represent this mooring. Time filtering was performed with an order 4 Butterworth lowpass filter (Roberts and Roberts, 1978).

Table 1. Mooring details and statistics for current meters in the 4-year time series (upper panel), and functioning time chart for each current meter (lower panel)

Mooring	Position	Days of record	Depth (m)		Mean of Velocity		Temperature (°C)
			Water	RCM	Magnitude (cm s^{-1})	Direction (deg)	
No. 1	71°30′N	467	227	50	4.3	123	6.5
	19°47′E	659		125	3.8	129	6.2
		834		212	3.9	134	5.8
No. 2	72°00′N	865	309	50	4.3	123	6.5

No. 2	72°00′N	865	309	50	4.3	123	6.5
	19°39′E	872		125	4.4	131	5.9
		624		225	4.0	134	5.7
		1077		294	3.5	139	4.9
No. 2b	72°15′N	199	324	50	2.2	66	6.5
	19°35′E	368		125	2.0	24	5.8
		199		225	2.8	55	5.7
		567		310	2.7	50	4.5
No. 3	72°30′N	905	388	50	3.4	120	6.1
	19°32′E	908		125	3.5	117	5.7
		1060		225	3.6	114	5.2
		1280		375	3.2	101	3.1
No. 3b	72°45′N	275	392	50	2.5	141	5.3
	19°32′E	171		125	4.4	155	5.1
		171		385	3.4	171	2.9
No. 4	73°00′N	657	419	50	2.2	124	5.8
	19°33′E	1194		125	2.6	113	5.3
		543		225	2.1	118	4.2
		705		401	0.8	130	2.3
No. 5	72°30′N	414	480	50	1.7	190	4.9
	19°20′E	1082		125	1.9	209	4.2
		715		225	5.0	224	3.2
		1082		464	7.8	227	1.5

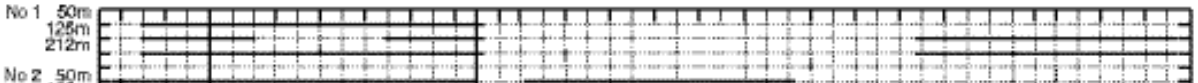
No 1 50m
125m
212m
No 2 50m

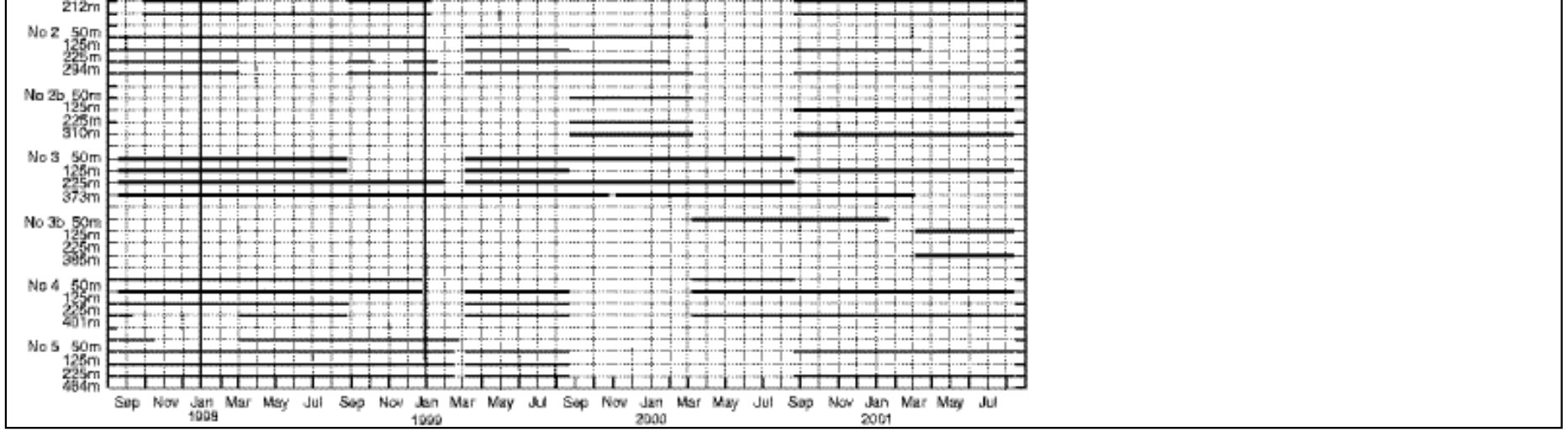

The presence of mesoscale eddies (with time scales of several days) can seriously alias the result when calculating volume fluxes from moored current meters, but as shown in Appendix A the influence of mesoscale activity in this area is relatively small when investigating fortnightly or longer time scales. Based on this, the time series were filtered by removing fluctuations with periods less than 14 days prior to further analysis.

Transports between 71°15′N and 73°45′N were calculated by assigning a rectangle surrounding each current meter. The volume fluxes were calculated from the daily values of the cross-sectional current component (which is the east–west component as the section is aligned north–south). For the period January–February 1999, there were only a few instruments working (Table 1). Fortunately, the bottom RCM7 at mooring No. 3 worked for the entire period, as earlier this location was found to be the representative for the total flow through the section (Ingvaldsen et al., 2002). A linear relationship between the velocities from the available instruments and the total flux was assumed, and regression analysis for the period of August 1997–December 1998 was used to express the total transport and to estimate the flux from January–February 1999. The same method was used for the periods with only three moorings (September 1999–August 2000, see Table 1). Due to the barotropic structure of the currents, the expression for total volume flux was based on the two deepest instruments on the three moorings. The regression analysis was performed for the period of September 2000–August 2001. When error estimates are assigned to the volume fluxes, the calculations were performed as described in Appendix B.

The current meter data is extended with data from two moorings that were deployed on the shelf south of Svalbard (Fig. 2). One mooring (No. 6) was deployed at 73°45′N in the period of August–October 1997 and had RCM7 current meters deployed in 50 and 125 m depths. The other mooring (No. 6b) was deployed at 74°00′N in the period of August 1998–March 1999 and had RCM7s deployed in 50 and 106 m depths. The settings and processing of the data were identical to the 4-year series of the current measurements. A small data set sampled after the 4-year period is also included in this paper. For the period of August 2001–March 2002 a mooring with an Aanderaa profiling Doppler Current Meter 12 (DCM12) and a RCM7 was deployed at 73°30′N. The DCM12 was deployed in a depth of 45 m and measured velocity in five bins between 5 and 41 m every second hour, while the RCM7 was deployed in a depth of 60 m.

The section between Norway and Bear Island is a standard hydrographic section and is sampled 6 times a year by the Institute of Marine Research, Norway. Here, salinity and temperature from the period 1997–2001 is used.

The wind field at 10 m above sea level was taken from the Norwegian Meteorological Institute (Met.no) hindcast archive (updated from Eide et al., 1985), while the sea level height was obtained from numerical simulations that were carried out by the use of NORWECOM (Skogen and Søiland, 1998). NORWECOM is a 3D, primitive equation, sigma-coordinate coastal ocean model based on the Princeton Ocean Model (Blumberg and Mellor, 1987). The model domain covered the Nordic Seas, the Barents Sea and the Arctic Ocean. The model was discretized on a 20 km horizontal polar stereographic grid, and forcing included initial and boundary conditions from The Norwegian Meteorological Institute-Institute of Marine Research diagnostic climatology (Engedahl et al., 1998), realistic meteorological forcing from the NCEP-NCAR reanalysis project, and monthly mean river runoff and tidal forcing. The model has been validated for the Nordic and Barents Sea (Asplin et al., 1998), and the results showed that the produced velocity fields, in general, are qualitatively good, but the magnitudes are underestimated. Based on this we expect the sea level height to be realistic but with possible underestimated gradients.

Throughout the paper *winter* will denote the months of December through March, and *summer* June through August.

3. Results

The climate of the Barents Sea varies with both long- and short-term quasi-regular fluctuations (Fig. 3). Ådlandsvik and Loeng (1991) found an agreement of the fluctuations in many of the climatic variables in the Barents Sea. They suggested that the climate of the Barents Sea oscillates between a warm and a cold state. Positive feedback mechanisms maintain the states, i.e. they are stable states. The transition from one state to the other is likely to be enforced externally by variations in larger-scale oceanic and atmospheric circulation (Ådlandsvik and Loeng, 1991). The current measurement programme started in a climatically cold state (Fig. 3), but in late winter/early spring in 1998 the climate conditions changed to a warm state that lasted throughout the measurement period. This means that the first year of the measurements were sampled in a transition year, while the last 3 years were sampled during a warm state. The seasonal cycle does not have to be the same for a transition year and a stable state year. In this paper, we will focus on the stable state years, as these are most common.

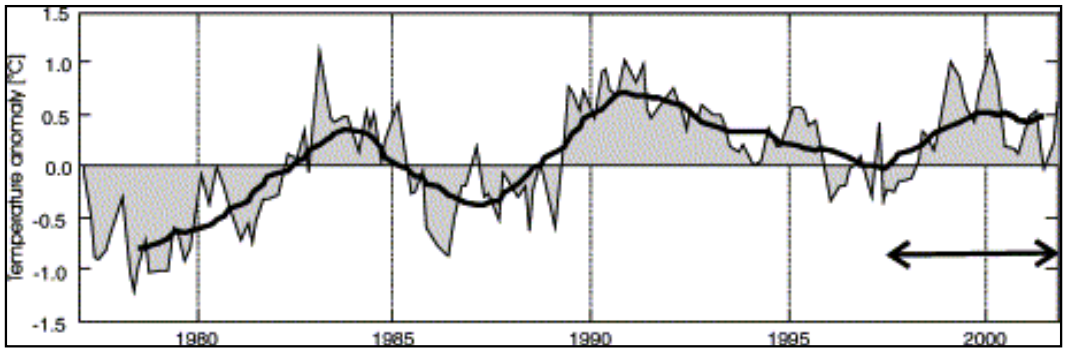

Fig. 3. Mean temperature anomaly in the AW at the section between Norway and Bear Island based on repeated sections of hydrography. The anomaly is calculated for the area between 71°30′N and 73°30′N, and between 50 and 200 m depth. The thick line shows the 3-year running mean, and the black arrow shows the period when the current meter moorings were deployed.

The mean salinity distribution in January and August (Fig. 4) reveal that the moorings generally captured the main part of the Atlantic inflow (identified by the 35 psu isoline), although some parts are missing, especially in the south during summer and in the upper 50 m during winter. Motivated by the available data sets (basically the location of the moorings), the section was divided into four regions (Fig. 4). The seasonal signal of each region is investigated and an attempt to quantify the transport of AW is also made.

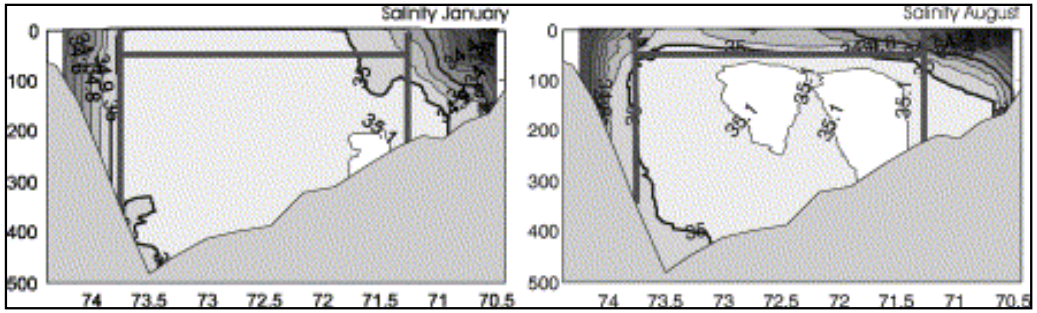

Fig. 4. Mean salinity in January and August for the period 1997–2001. The thick lines separate the four regions of investigation.

3.1. Region 1—the area occupied by the moorings

The moorings covered the area between 71°15′N and 73°45′N and from 50 m depth to the bottom. The quality of the salinity data from the RCM7 s was poor, and an identification of the different water masses in the flow by temperature and salinity could not be made. Thus, AW was defined by temperature as water above 3°C.[1] Concerning the seasonal cycle, three features of the monthly mean transports are striking (Fig. 5a). The first is a transport minimum in spring (March–April). The second is the apparent lack of a clear seasonal cycle with higher inflow during the winter than in the summer. However, when separated into different moorings it is evident that there are several contradicting seasonal cycles within the section (Fig. 5b–d). In the northern part of the section there is a seasonal cycle with an outflow of AW during winter and an inflow during summer, although there are big year-to-year differences in the monthly means in this area. The middle part has a weak seasonal cycle with a higher inflow during winter, while the southern part has a very stable inflow without any seasonal signal at all. Due to its high stability, the southernmost mooring has the highest mean inflow of AW, although it in general has the weakest velocities. The third feature is that the first year of the measurements showed high inflow compared to the others (Fig. 5a), and substantial differences appear if the seasonal mean total transports are calculated separately for the first and for the last 3 years (Table 2). The first year had an abnormally high inflow especially during summer compared to the remainder of the time series. As already mentioned this year was a transition year between two states, which indicates a strong external forcing. Note also that if the first year of the measurements is not included, the year-to-year differences in the monthly means of the total transport are reduced (Fig. 5a). Based on the preceding discussion, we propose that the first year of the measurements is not likely to be representative for the stable state (or most usual) seasonal cycle. The most realistic estimate of the AW transport between 71°15′N and 73°45′N and 50 m to bottom for a normal year is therefore 1.5 Sv (1 Sv=10^6 m^3 s^{-1}) during winter and 1.1 Sv during summer. The annual mean is 1.2±1.1 Sv.

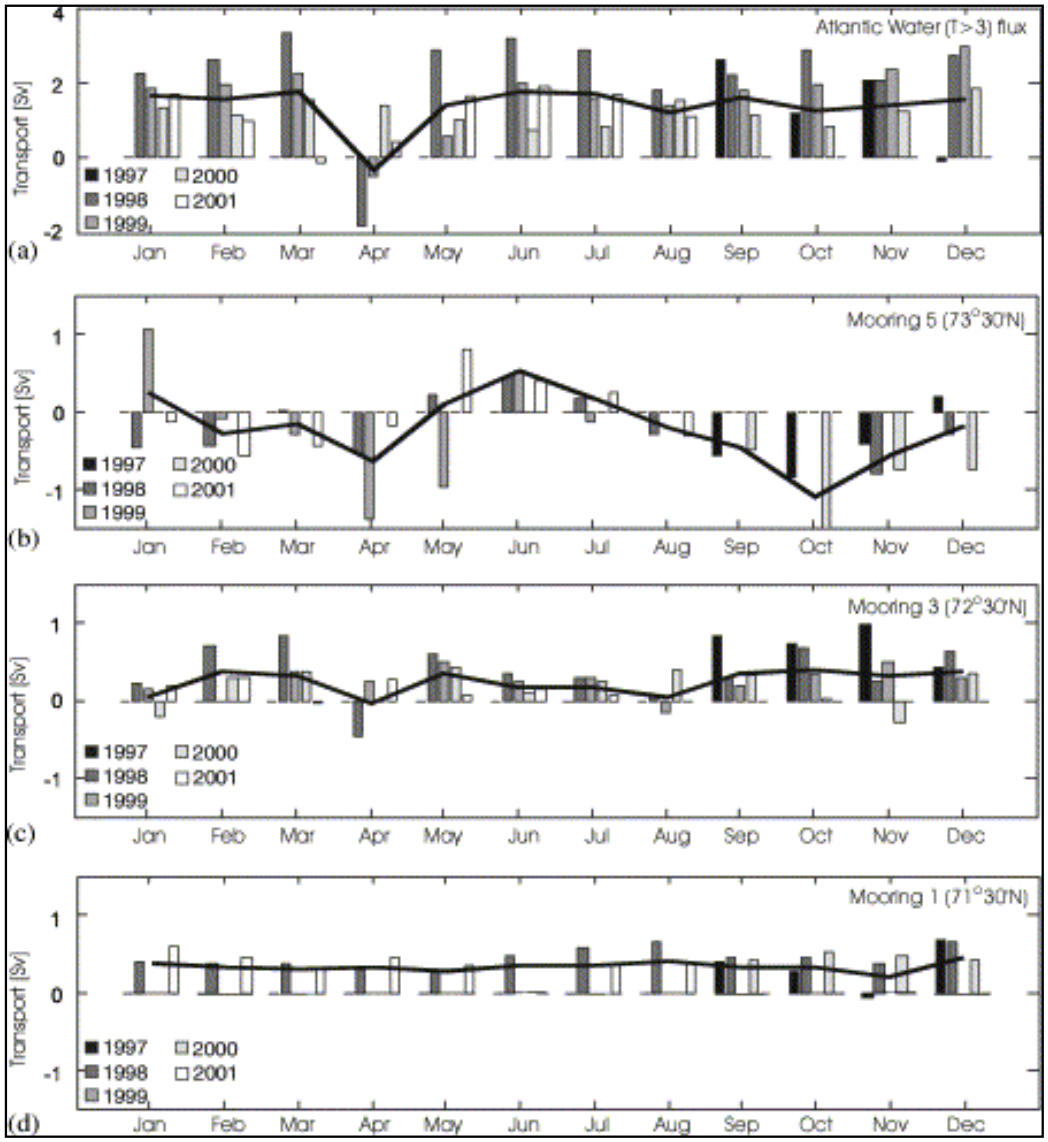

Fig. 5. Monthly mean transport of AW estimated from (a) all moorings, and (b–d) the separate contribution from three of the moorings. Positive transport is into the Barents Sea (i.e. eastwards).

Table 2. Mean transports and error estimates from current measurements separated in the first and the last 3 years. The calculations of the error estimates were performed as described in Appendix B

	Atlantic Water	
	Winter	Summer
Mooring area, Sep 97–Aug 98	1.7 ± 4.1	2.1 ± 3.0
Mooring area, Sep 98–Aug 01	1.5 ± 1.9	1.1 ± 1.8

3.2. Region 2—the upper 50 m above the moorings

The mean salinity distributions during summer and winter show a clear seasonal signal in this area (Fig. 4). During winter the AW is present all the way to surface, while during summer the stratification is strong and by the end of summer no AW is present in the upper 50 m. To estimate the transport of AW, we investigate whether the direct wind drift in the upper meters gives a significant contribution. The instantaneous and vertically integrated Ekman transport has a cross-sectional component U_E given by

$$U_E = \frac{1}{\rho_0 f}\tau^y,$$

where ρ_0 (1026 kg m^{-3}) is the density of seawater and f (1.39×10^{-4} s^{-1}) is the Coriolis parameter. τ^y, the along-sectional wind stress, was obtained from the along-sectional wind velocity $\vec{v}$ by

$$\tau^y = \rho_{air} C_d |\vec{v}| \vec{v},$$

where ρ_{air} (1.3 kg m^{-3}) is the density of air and C_d is the drag coefficient as given by Large and Pond (1981). The wind data are provided on a regular grid, and the grid points lying closest to the section were identified. To determine the integrated transport a rectangle surrounding each point was assigned. Although the Ekman transport on a daily time scale varied between 1.5 Sv into the Barents Sea and 1.6 Sv out, the variability was high and the resulting mean values were close to zero. The mean values were 0.02 Sv during winter and 0.00 during summer with a long-term mean of 0.01, i.e. negligible considering our accuracy.

Another method for estimating the transports in the upper 50 m is to extrapolate the velocity from the current meter in 50 m depth to the surface. To investigate the reliability of this method, transport estimates from a profiling current meter DCM12 and a RCM7 deployed in 60 m were compared. Volume transports in the upper 50 m were estimated by five bins from the DCM12, and by letting the RCM7 represent the top 50 m (Fig. 6a). The results show surprisingly small differences, both for amplitude and

phase (the correlation coefficient is 0.91). These measurements were done mainly during fall and winter, when the stratification is weak and the winds are strong. During summer the strong stratification may prevent such a vertical homogeneity, and it seems as if the fit between the DCM12 and the RCM7 is weaker in early fall when the upper waters are still stratified (Fig. 6a). However, the good comparison with the DCM12 justifies a simple extrapolation of the observations from 50 m depth to the surface. The transport in the upper 50 m was therefore calculated from the instruments in 50 m depth and the resulting mean total transports were 0.25 Sv both for summer and winter. To quantify how much of the flux is AW, we noted that AW covers an area of about 75% of the box during winter (Fig. 4), thus giving an AW inflow of (using January as a representative) 0.18 ~0.2 Sv. Taking August as a representative for summer the transport of AW is ~0.0 during summer (Fig. 4).

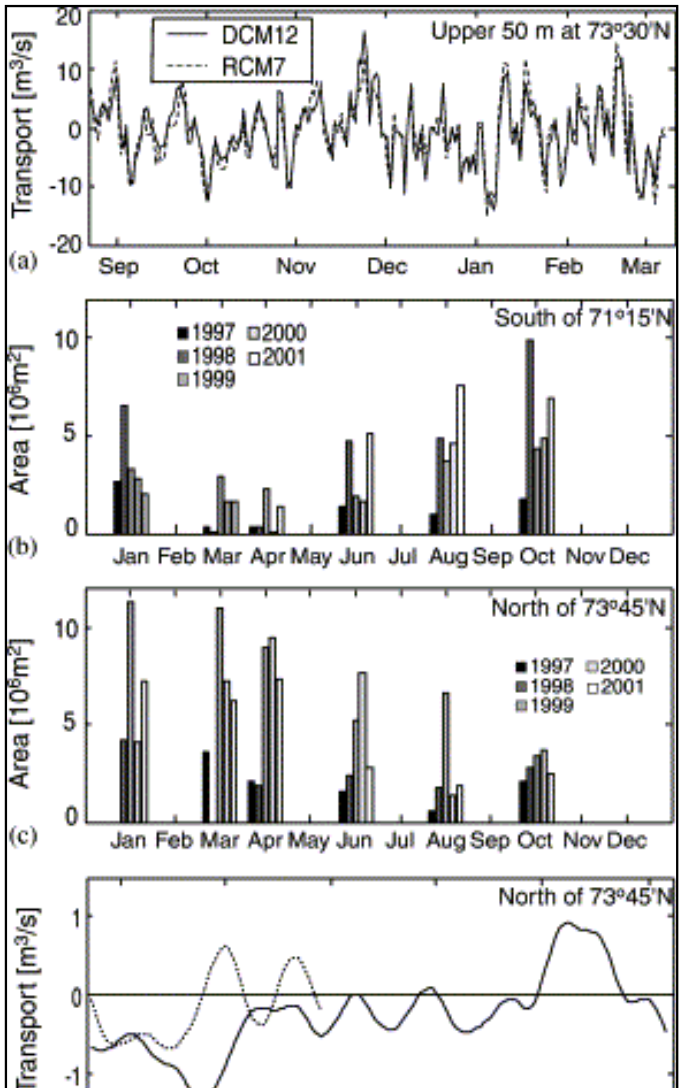

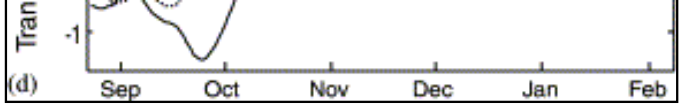

Fig. 6. Calculation of volume fluxes in the regions shown in Fig. 4. (a) Volume flux between the surface and 50 m depth estimated by both a profiling current meter DCM12 and by extrapolating a RCM7 deployed in 60 m. (b) The area occupied by AW for each repetition of the standard section in the period 1997–2001 south of 71°15′N, and (c) north of 73°45′N. (d) Volume flux north of 73° 45′N estimated from the mooring at 73°45′N in August–October 1997 (⋯), and from the mooring at 74°00′N in August 1998–February 1999 (—).

3.3. Region 3—the area south of 71°15′N

The mean salinity distribution shows that the Atlantic inflow is pushed down-slope away from the Norwegian coast during the winter compared to the summer (Fig. 4). The calculated area occupied by AW (defined by S>35 and T>3°C) reveals this feature clearly with a much smaller amount of AW present in late winter and spring than in summer (Fig. 6b).

Considering the transports in this area, Blindheim (1989) presented a 2-month time series of current meters between Norway and Bear Island, and a rough estimate of the volume transport south of 71°15′N based on his results give a flux of 0.7 Sv into the Barents Sea. Approximately 0.5 Sv of this was the NCC, leaving 0.2 Sv of Atlantic water inflow. The measurements were from the period of September–October, i. e. likely to be representative for the summer situation due to the stratification. The current measurements of Blindheim (1989) indicated also a flow with only weak horizontal gradients between 71°30′N and the NCC. A rather crude estimate of the transport of AW is therefore to multiply the area occupied by AW with a constant velocity. Our southernmost mooring revealed seasonally stable currents (Fig. 5d), with a long-term mean velocity of about 3.5 cm s^{-1}. This gives Atlantic transports of 0.08 Sv during winter and 0.13 Sv during summer. If the constant velocity is increased to 5 cm s^{-1}, the transports become ~0.13 Sv during winter and ~0.21 Sv during summer. These estimates are in good agreement with the number obtained by Blindheim (1989). As it is likely that this method underestimates the AW flux, our "best guess" is that the Atlantic transport in this area is ~0.1 Sv during winter and ~0.2 Sv during summer.

3.4. Region 4—the area north of 73°45′N

The area north of 73°45′N occupied by AW was computed as in the previous section. In contradiction to what was found in the south, these results shows that the Atlantic influence is stronger during the winter and spring than during the summer (Fig. 6c). Thus, the Atlantic domain is displaced northwards during winter. As was shown earlier, the mooring at 73°30′N had a clear seasonal cycle with inflow during the

summer and outflow during the winter (Fig. 5b), indicating that the AW found north of 73°45′N during the winter is recirculating water.

Two moorings have been deployed on the slope south of Bear Island, one at 73°45′N, the other at 74°00′ N (Fig. 2). Unfortunately, none were deployed during summer. By allowing each of the moorings to represent the total area north of 73°45′N, two time series of (total) transport are obtained (Fig. 6d). Although most of the time the flow was out of the Barents Sea at these locations, persistent inflow for almost 1 month occurred. The mean Atlantic transports were −0.1 Sv for both moorings.

As another approach, the area occupied by AW was multiplied by a constant velocity as was done in the previous section. The mean velocity of the two upper instruments at mooring no. 5 were taken as representative for the velocity in the AW also north of 73°45′N. The velocities were about 2 cm s^{-1} westward during winter and 1.5 cm s^{-1} eastward during summer. The calculated volume fluxes of AW become −0.1 Sv during winter and ~0.0 Sv inflow during summer, i.e. in reasonable agreement with the two moorings on the slope.

4. Discussion

The results from the previous sections are summarized in Fig. 7. The results reveal an Atlantic transport of 1.7 Sv during winter and 1.3 Sv during summer. This gives a seasonal variation of 25%, although an abnormally strong flow in some years may differ substantially from these values. The annual mean is 1.5 Sv. The volume flux in the area occupied by the moorings is by far the largest contribution to the total flux, which means that the moorings captured most of the Atlantic inflow. This is probably realistic, although its importance may be exaggerated due to the rather crude calculation methods used outside the mooring domain. However, independent of the quantification of the actual transports, the 4-year records from the current meters and the hydrography revealed a seasonal cycle in both the current velocities and the distribution of AW within the section. The main findings are that there is a pronounced minimum in Atlantic inflow or even an outflow in the spring (Fig. 5), there is, in general, higher Atlantic inflow during winter than summer (Table 2 and Fig. 7), the seasonal variation within the section is not uniform (Fig. 5), and the Atlantic domain is displaced northwards during the winter compared to the summer (Fig. 6 and Fig. 7).

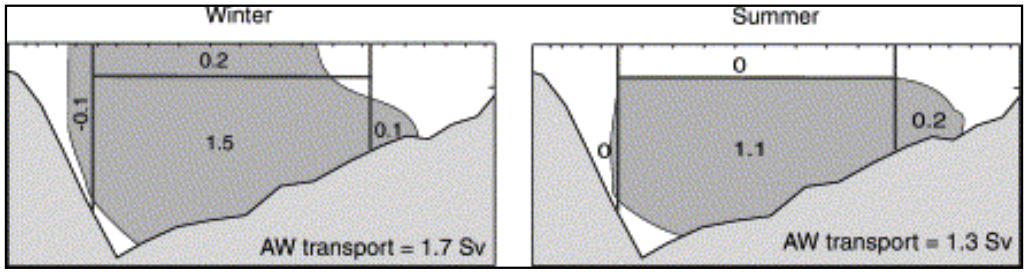

Fig. 7. Schematics of the distribution of AW within the BSO and the estimated volume fluxes in the different regions.

4.1. The spring minimum

The current measurements revealed a pronounced minimum in spring (Fig. 5). At times it was even an outflow, being persistent as it shows on the monthly mean transports. From a separate investigation of the velocity fields, Ingvaldsen et al. (2004) found that the relatively strong outflows in the northern part of the BSO were generated by northerly winds. This suggests that the spring minimum is connected to a seasonal shift in the along-sectional (north–south) wind field. The winds in the section (Fig. 8) are part of a pronounced spring phenomenon with a periodic wind change from the general southerly direction to a northerly. Similar shifts in the winds are occurring in most of the Barents Sea (not shown). The northerly winds move large amounts of water from the Arctic to the northern and eastern Barents Sea, therefore pushing the water masses of the northern and eastern Barents Sea southwards. The supply of water into the Barents Sea from the Arctic Ocean and a southward movement of the water masses of the northern and eastern Barents Sea can explain why the large outflows can be present at the BSO without violating the volume balance of the Barents Sea. It is also consistent with the necessity for a response time between wind and sea level for such a large-scale movement.

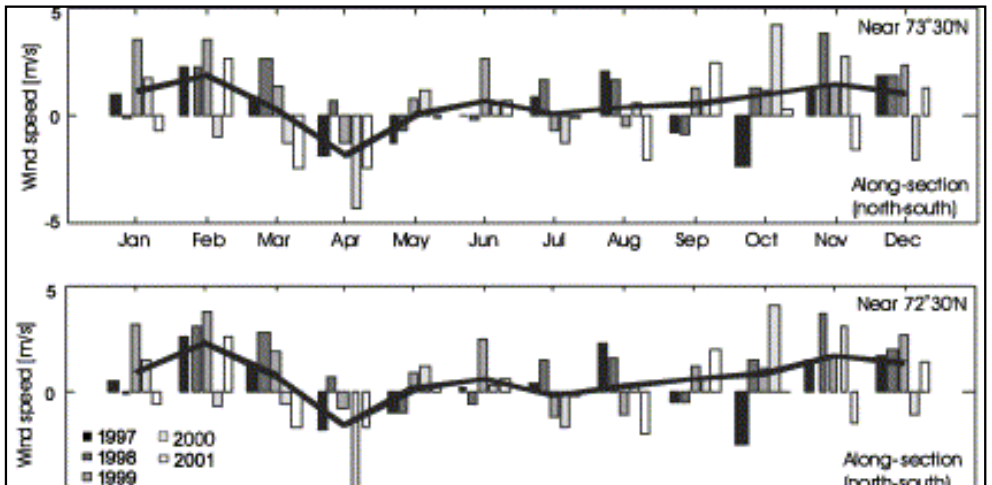

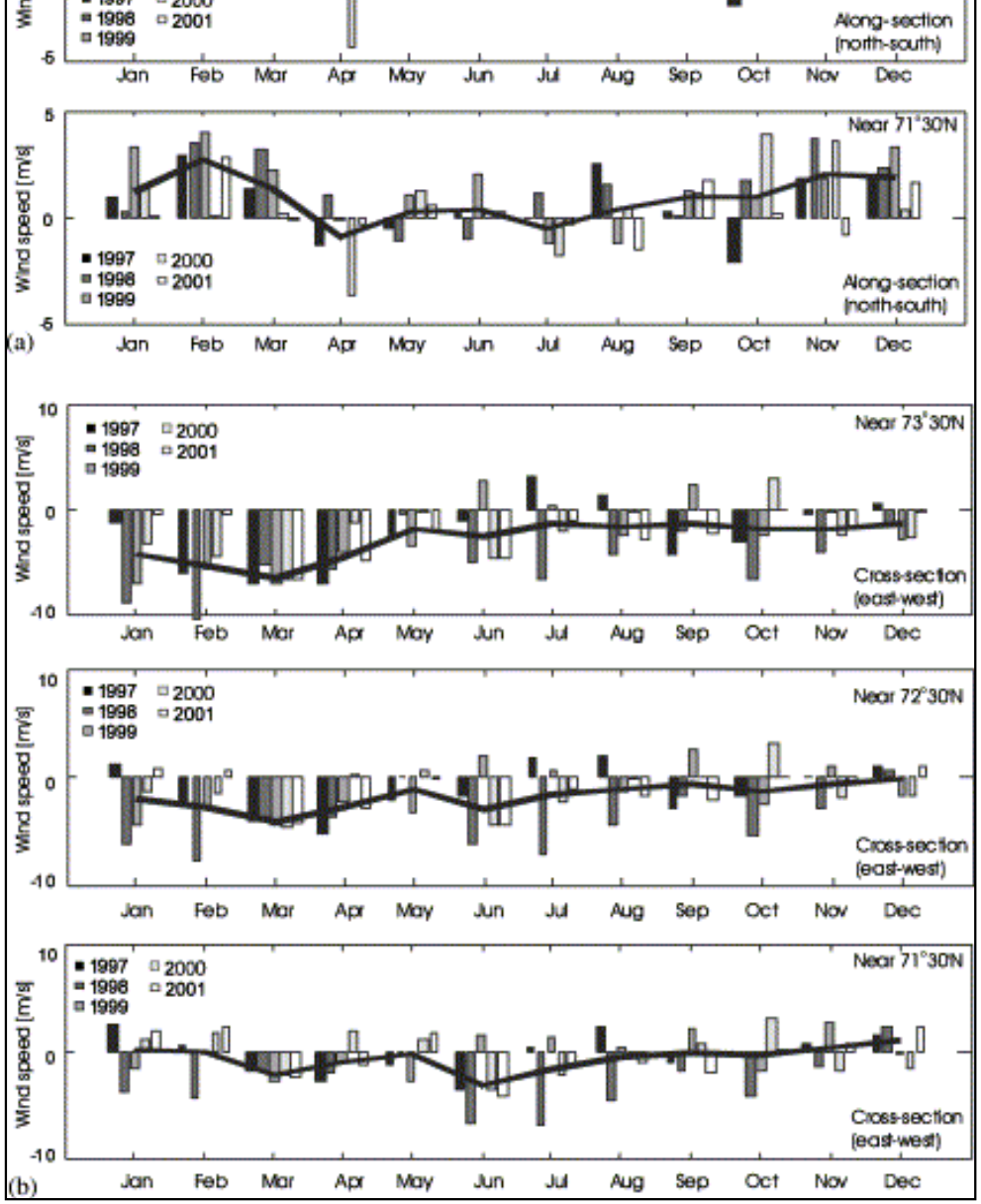

Fig. 8. Monthly mean (a) along-sectional (north-south), and (b) cross-sectional (east–west) wind speed at locations near the moorings. Southerly and westerly winds are positive (i.e. positive directions are northwards and eastwards).

Additional factors may also contribute to the spring outflows. One of these is the effect of the vertical stratification; as the stratification is almost absent in spring, the effect of the wind will reach further down in the water column. Furthermore, the formation of high-density water during the winter as described by Midttun (1986) may enhance the observed outflow. Although the outflows have too high temperatures to

be a draining of this winter water, the ongoing process of production of winter water will generate baroclinic horizontal pressure gradients towards the west that will increase during winter. However, due to the barotropic nature of the currents, the sea level should be expected to be important. In other words, the large spring outflows are caused by an annual spring event of northerly winds, but there are probably several (not fully understood) contributing processes.

4.2. Higher inflow during winter than summer

The higher inflow during winter is partly due to the presence of AW in the top 50 m, but is mainly due to higher current velocities below the direct wind-driven layer (Fig. 7). There are (at least) two aspects that can be responsible for the higher inflow in the deeper part during the winter; the NAC is stronger due to upstream conditions (Orvik et al. (2001) found that the eastern branch of the NAC in the Norwegian Sea has a systematic annual cycle which doubles the inflow during winter), and/or there may be local effects in the BSO that amplifies the current. In the following, we will try to identify which of the two aspects that are dominating.

As shown by Ingvaldsen et al. (2004), the main process that drives the currents of the Atlantic inflow are sea-level changes within the section that are induced by Ekman transport. The Ekman transport is limited to the upper layers and its direct contribution to the total transport is comparatively small (e.g. Section 3.2), but it has a significant effect through its ability to accumulate water and change the sea level. The pressure gradient associated with the sea-level gradient then drives barotropic currents. The Ekman transport affects the sea level in two ways. Along a coastline a uniform alongshore wind will increase or decrease the water level directly within a distance of the barotropic Rossby radius of the coast (e.g. Gill, 1982), while away from the boundaries, the shear in a non-uniform wind field will result in local accumulation or removal of surface waters. To investigate the effect of the shear of the local wind field we use the *along-sectional* Ekman transport V_E given by

$$V_E = -\frac{1}{\rho_0 f}\tau^x.$$

The cross-sectional wind stress τ^x is obtained from the cross-sectional wind velocity $\vec{u}$ by $\tau^x = \rho_{air} C_d |\vec{u}| \vec{u}$ (the other variables are defined as in Section 3.2). The sea level at any given point depends on the amount of water transported into and out of the area. Therefore, the net Ekman transport in a given area was calculated as the difference between the two surrounding points in the north and south. At the Norwegian coast, there can be no Ekman transport across the coast and V_E was defined as zero.

During the winter the wind field is clearly sheared and will decrease the water level along all of the section except near the coastline (Fig. 9), while during the summer it is only in the southern part that there is an effect of the wind shear. Note that due to the remotely forced NAC the water level, in general, is higher towards the Norwegian coast, i.e. the wind field will only modify an existing gradient. The wind field, Ekman transports and the consequences for the sea level are outlined in Fig. 10. This reveals that due to the local wind field the water-level gradient is much steeper during winter than that of summer, and the associated geostrophic currents are therefore stronger during winter. The cross-sectional geostrophic current U_{geo} is given by

$$U_{geo} = -\frac{g}{f}\frac{\partial \eta}{\partial y},$$

where η is the water level, g (9.82 m s^{-2}) is the acceleration due to gravity and f is the Coriolis parameter. The water level due to the local wind field is difficult to quantify as it depends on the along-sectional and the cross-sectional Ekman transports as well as Ekman pumping. However, the numerical model finds the mean total water level during summer and winter, and the associated geostrophic currents reveal the deduced seasonal variability with higher velocities during the winter than in summer (Fig. 11). The calculated currents include both the effect of the local wind and the possible stronger gradient due to a stronger NAC during winter. However, a stronger NAC during the winter should, at least in principle, give a uniform gradient along the section, while the difference between the geostrophic currents during winter and summer reveal non-uniformity that resembles the difference in the water-level gradients deduced from the shear of the wind field (Fig. 10 and Fig. 11, see also Section 4.3). This suggests that the higher inflow during the winter is mostly due to the shear in the cross-sectional wind, although possibly amplified by a seasonal cycle in the remotely forced NAC. To quantify the barotropic contribution, the volume flux is calculated by simply interpolating the barotropic geostrophic current (Fig. 11) all the way to bottom, giving 4.6 Sv during the winter and 3.1 Sv during the summer. Considering that the strong outflow in the deepest part of the channel is not included, and neither is the baroclinic flow contribution (and this is total transport, not only transports of AW), these numbers are reasonable. The seasonal variation is 33%, which is higher than the 25% found in the beginning of this section. This may be related to an opposing seasonal signal in the deep outflow or in the other contributions that are not included.

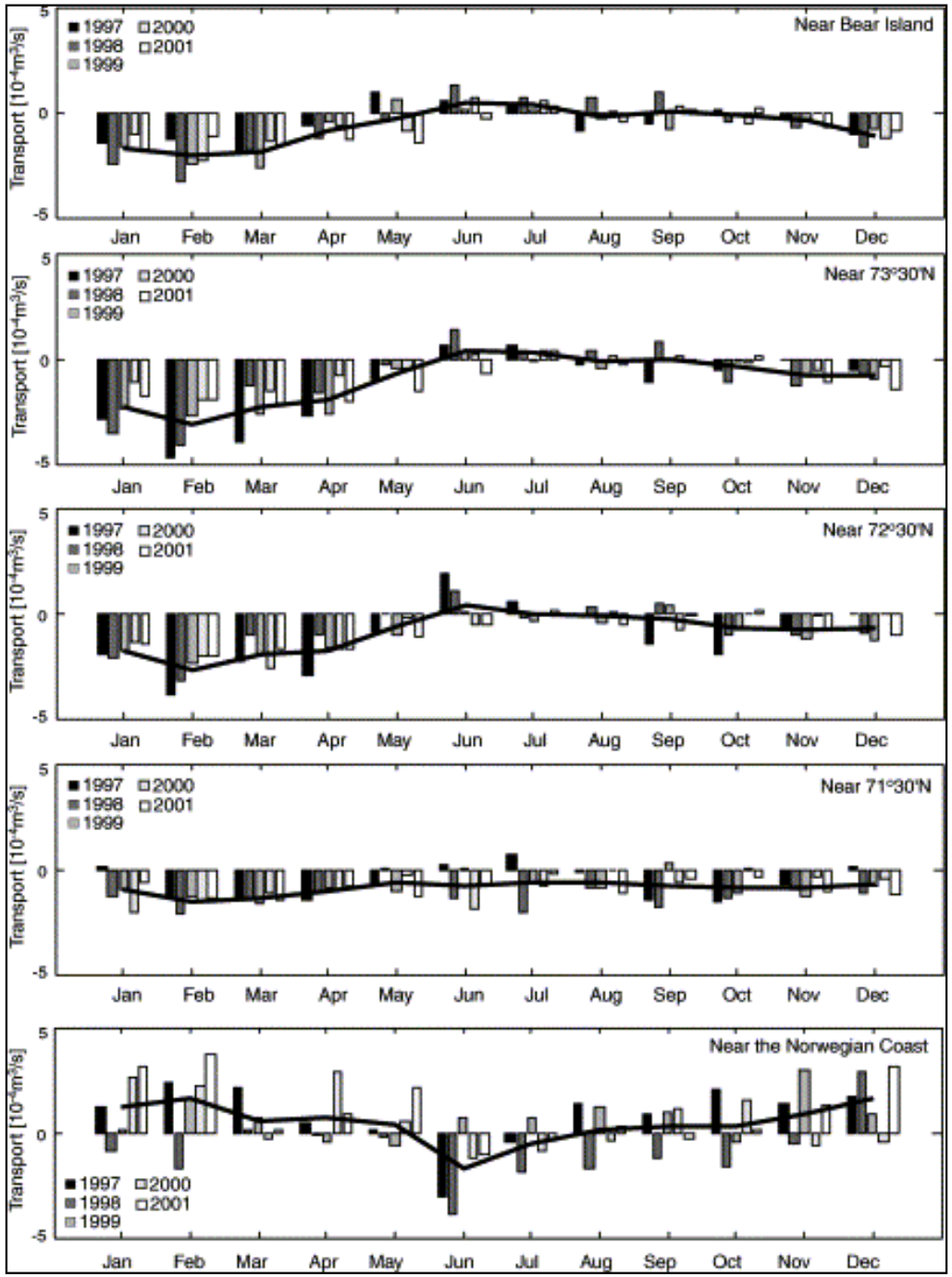

Fig. 9. Net along-sectional Ekman transport at the section between Norway and Bear Island. The calculation was performed so that the net transport is positive when the gain is larger than the lose, i.e. a negative transport is associated with a decrease in sea level.

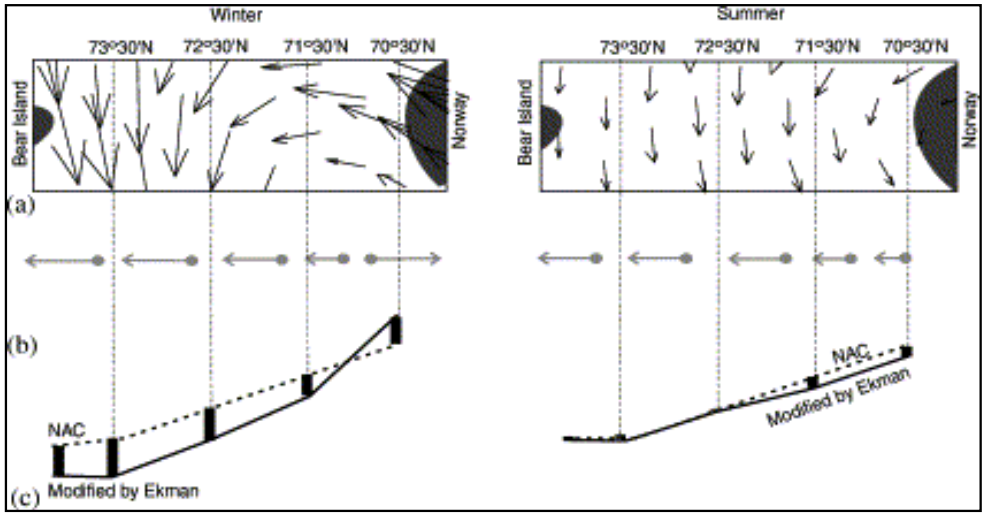

Fig. 10. (a) Horizontal view of the mean wind field at the BSO and (b) a sketch of the associated Ekman transport along the section. (c) Sketch of sea-level height (vertical view), where the dotted line denotes the sea level from the NAC, and the solid line the sea level after modified by the along-sectional Ekman transport. The vertical bars show the relative scale of the mean net Ekman transport.

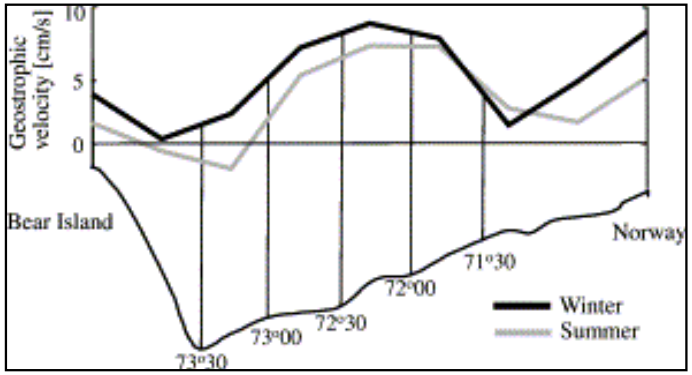

Fig. 11. Geostrophic velocity across the BSO during winter and summer calculated from the mean sea level.

4.3. The non-uniform seasonal variability within the section

The shear in the cross-sectional wind induces a non-uniform seasonal cycle within the section, which

resembles that in the geostrophic velocities (Fig. 10 and Fig. 11). The largest winter-to-summer differences in water-level gradient due to the shear of the wind field is found near the Norwegian coast (Fig. 10c), and this area also shows the largest winter to summer difference in geostrophic velocity (Fig. 11). Near 71°30′N alternatively, there is almost no difference between the seasons at all, which is also in accordance with the current measurement (Fig. 5). This shows the importance of the *shear* of the wind field, as both the wind speed and direction in this area changes substantially from winter to summer (Fig. 10a), but the net Ekman transport remains the same (Fig. 9 and Fig. 10). Therefore, the water level due to the shear of the wind will have almost the same gradient during both seasons (Fig. 10c), and the associated geostrophic current has no seasonal signal (Fig. 11). North of 72°00′N, the difference between winter and summer increases northward towards 73°30′N both for water-level gradient as expressed by the net Ekman transport (Fig. 10c) and geostrophic velocity (Fig. 11). A seasonal signal was also found in the current measurements in this area (Fig. 5). The geostrophic velocities do not reproduce the outflow in the northern part of the section (Fig. 11), reflecting that this probably not is driven by local sea-level gradients.

4.4. Seasonality in the distribution

The hydrographic data showed that the Atlantic domain, in general, is displaced northwards during the winter compared to that of the summer (Fig. 6 and Fig. 7). In the southern parts the Atlantic water is found further down-slope during the winter (Fig. 4). This is likely a result of coastal downwelling. The southwesterly winds along the Norwegian coast during the winter force the surface waters towards the coast (Fig. 10), and the water level along the Norwegian coast rise (consistent with the stronger geostrophic currents in Fig. 11). By continuity, the water masses of the deeper layer move offshore. This is consistent with the observed extent of the NCC, as being narrow and deep during the winter (illustrated by the 34.7 isoline in Fig. 4). During summer the winds are reversed but weaker, the Ekman transport is offshore and the NCC is wide and shallow (Fig. 4). The numerical model predicts a reduced water level at the Norwegian coast compared to the winter (Fig. 11). A seasonal lateral oscillation of the NCC forced by the Ekman transport of along-coast winds has earlier been reported off southern Norway (Sætre et al., 1998).

The results also showed a seasonal signal in the lateral distribution of AW in the northern parts (Fig. 6). The reason for this remains unknown, although it may be linked to stronger recirculation during the winter due to stronger winds.

5. Summary and conclusions

The seasonal cycle in the Atlantic inflow is examined using 4-year long records from moored current meters between 71°30′N and 73°30′N in the BSO, additional moorings north of 73°30′N, hydrographic measurements, wind, and sea level from a numerical model.

We find a seasonal cycle in both the transports and the distribution of AW within the section. The main findings are:

1. A higher Atlantic inflow during winter than summer is most common: This is connected to sea-level changes within the section induced by the shear of the cross-sectional wind field. The local wind field during winter is sheared, and through along-sectional Ekman transport, a relatively steep water-level gradient is created. The associated barotropic currents give a higher Atlantic inflow during the winter than the summer. The local wind field is probably capable of producing the observed seasonal variation, although it is possible that the remotely forced NAC also contributes. In years where the Barents Sea climate changes from a cold to a warm period (and probably vice versa), the seasonal cycle may be different.
2. The seasonal variation within the section is not uniform: This is connected to a non-uniform shear in the cross-sectional wind field. The middle and northern part of the section experiences a wind field with stronger shear during the winter than the summer, thereby giving a strong seasonal signal in these areas. Near 71°30′N on the other hand, the alluring result arises that both wind speed and direction change substantially from winter to summer, but the net Ekman transport does not. Therefore, the water-level gradient and the associated geostrophic current do not display any seasonal signal in this area.
3. The Atlantic domain is displaced northwards during the winter compared to the summer: In the south it is connected to coastal downwelling during the winter. The southwesterly winds give an Ekman transport onshore, the water level along the Norwegian coast is raised, and coastal downwelling moves AW down-slope away from the coast.
4. A pronounced minimum in Atlantic inflow or even an outflow in the spring: The situation is forced by an annual spring event of northerly (along-sectional) winds. The transport of AW across the section is quantified and reveals an Atlantic flow of 1.7 Sv during the winter and 1.3 Sv during the summer. This gives a seasonal variation of 25%, although abnormally strong flow in some years may differ substantially from these values. The annual mean transport of AW is found to be 1.5 Sv.

Acknowledgements

We would like to thank Peter Haugan for fruitful discussions and valuable comments on the manuscript. We are also grateful to the reviewers for valuable improvements of the manuscript. The results presented have partly been obtained through funding from the European Union MAST III VEINS programme and

the MAIA project. In addition, funding has come from the Research Council of Norway through the projects "Variation in space and time of cod and other gadoids: the effect of climate and density dependence on population dynamics" and NOClim.

References

Aagaard, K. and Woodgate, R.A., 2001. Some thoughts on the freezing and melting of sea ice and their effects on the ocean. *Ocean Modelling* **3**, pp. 127–135.

Ådlandsvik, B. and Loeng, H., 1991. A study of the climatic system in the Barents Sea. *Polar Research* **10** 1, pp. 45–49.

Asplin, L., Ingvaldsen, R., Loeng, H., Ådlandsvik, B., 1998. Description and validation of a 3-dimensional numerical model of the Nordic and Barents Seas. Fisken og Havet, 10, Institute of Marine Research, Norway, p. 35.

Blindheim, J., 1989. Cascading of Barents Sea bottom water into the Norwegian Sea. *Rapports et Proces-verbaux Réunions Conseil permanent International pour l'Exploration de la Mer* **188**, pp. 49–58.

Blindheim, J., Toresen, R., Loeng, H., 2001. Fremtidige klimaendringer og betydningen for fiskeressursene, Fisken og Havet, 2, pp. 73–78 (in Norwegian).

Blumberg, A.F., Mellor, G.L, 1987. A description of a three-dimensional coastal ocean model. In: Heaps, N. (Ed.), Three-Dimensional Coastal Models, Vol. 4. American Geophysical Union, Washington, DC, pp. 1–16.

Eide, L., Reigstad, M., Guddal, J., 1985. Database av beregnede vind og bølgeparametere for Nordsjøen, Norskehavet og Barentshavet hver 6. time for årene 1955–1981. Technical Report, The Norwegian Meteorological Institute, Oslo/Bergen, p. 38.

Engedahl, H.B., Ådlandsvik, B. and Martinsen, E., 1998. Production of monthly mean climatological archives for the Nordic Seas. *Journal of Marine Systems* **14**, pp. 1–26.

Fachbach, E., Meincke, J., Østerhus, S., Rohart, G., Schauer, U., Tverberg, V. and Verduin, J., 2001. Direct measurements of volume transports through Fram Strait. *Polar Research* **20** 2, pp. 217–224.

Furevik, T., 1998. On the Atlantic Water flow in the Nordic Seas: Bifurcation and Variability. Ph.D. Thesis, University of Bergen, Norway, p. 218.

Gill, A.E., 1982. *Atmosphere-ocean Dynamics*, Academic Press, San Diego, CA, USA p. 662 .

Giske, J., Skjoldal, H.R. and Slagstad, D., 1998. Ecological modelling for fisheries. In: Rødseth, T., Editor, , 1998. *Models for Multispecies Management*, Physica-Verlag, Wurzburg, pp. 11–68.

Harms, I.H., 1992. A numerical study of the barotropic circulation in the Barents and Kara Seas. *Continental Shelf Research* **12** 9, pp. 1043–1058.

Haugan, P., 1999. On the transports of mass, heat and carbon in the Arctic Mediterranean. Ph.D. Thesis, University of Bergen, Norway, p. 166.

Ingvaldsen, R., Loeng, H. and Asplin, L., 2002. Variability in the Atlantic inflow to the Barents Sea based on a one-year time series from moored current meters. *Continental Shelf Research* **22**, pp. 505–519.

Ingvaldsen, R.B., Asplin, L., Loeng, H., 2004. The velocity field in the western entrance to the Barents Sea, Journal of Geophysical Research, in press.

Large, W.G. and Pond, S., 1981. Open ocean momentum flux measurements in moderate to strong winds. *Journal of Physical Oceanography* **11**, pp. 324–336.

Loeng, H., Sætre, R., 2001. Features of the Barents Sea Circulation. Fisken og Havet, 1, Institute of Marine Research, Norway, p. 40.

Loeng, H., Ozhigin, V., Ådlandsvik, B., Sagen, H., 1993. Current measurements in the northeastern Barents Sea. ICES C.M.1993/C:41, 22pp.

Loeng, H., Ozhigin, V. and Ådlandsvik, B., 1997. Water fluxes through the Barents Sea. *ICES Journal of Marine Science* **54**, pp. 310–317.

Midttun, L., 1986. Formation of dense bottom water in the Barents Sea. *Deep-Sea Research* **32**, pp. 1233–1241.

O'Dwyer, J., Kasajima, Y. and Nøst, O.A., 2001. North Atlantic Water in the Barents Sea Opening, 1997

to 1999. *Polar Research* **20** 2, pp. 209–216.

Orvik, K.A., Skagseth, Ø. and Mork, M., 2001. Atlantic inflow to the Nordic Seas: current structure and volume fluxes from moored current meters, VM-ADCP and SeaSoar-CTD observations 1995–1999. *Deep-Sea Research I* **48**, pp. 937–957.

Ottersen, G and Loeng, H., 2000. Covariability in early growth and year-class strength of Barents Sea cod, haddock and herring: the environmental link. *ICES Journal of Marine Science* **57**, pp. 339–348.

Ozhigin, V.K., Ushakov, N.G., 1985. The effect of the thermal conditions of the sea and atmospheric circulation on the distribution of the Barents Sea capelin feeding areas. In: Gjøsæter, H. (Ed.), Proceedings of the Soviet–Norwegian Symposium, Murmansk, 26–28 May 1985, Institute of Marine Research, Norway, pp. 149–156.

Parsons, A.R., 1995. On the Barents Sea Polar Front in summer and interpretations of the associated regional oceanography using an Arctic Ocean general circulation model. Ph.D. Thesis, Naval Postgraduate School Monterey, California, p. 185.

Roberts, J. and Roberts, T.D., 1978. Use of Butterworth low-pass filter for oceanographic data. *Journal of Geophysical Research* **83**, pp. 5510–5514.

Rudels, B., 1987. On the mass balance of the Polar Ocean, with special emphasis on the Fram Strait, p. 53, Norsk Polarinstitutt Skrifter 188.

Rudels, B., Jones, B., Anderson, L., Kattner, G., 1994. On the intermediate depth waters of the Arctic Ocean. In: Johannessen, O., Muench, R., Overland, J. (Eds.), The Polar Oceans and Their Role in Shaping the Global Environment: The Nansen Centennial Volume, Vol. 85. Geophysical Monograph, American Geophysical Union, Washington, DC, pp. 33–46.

Schauer, U., Muench, R., Rudels, B. and Timokov, L., 1997. Impact of eastern Arctic shelf waters on the Nansen Basin intermediate layers. *Journal of Geophysical Research* **102**, pp. 3371–3382.

Schauer, U., Loeng, H., Rudels, B., Ozhigin, V.K. and Dieck, W., 2002. Atlantic Water flow through the Barents and Kara Seas. *Deep-Sea Research I* **49**, pp. 2281–2298.

Schauer, U., Rudels, B., Jones, E.P., Anderson, L.G., Muench, R.D., Bjørk, G., Swift, J.H., Ivanov, V. and Larsson, A.-M., 2002. Confluence and redistribution of Atlantic water in the Nansen, Amundsen and

Marakov basins. *Annales Geophysicae* **20**, pp. 257–273.

Skjoldal, H.R. and Rey, F., 1989. Pelagic production and variability of the Barents Sea ecosystem. In: Sherman, K. and Alexsander, L.M., Editors, 1989. *Biomass Yields and Geography of Large Marine Ecosystems, American Association for the Advancement of Science, Selected Symposium III*, Westview Press, Boulder, CO, USA, pp. 241–286.

Skjoldal, H.R., Gjøsæter, G. and Loeng, H., 1992. The Barents Sea ecosystem in the 1980s: ocean climate, plankton, and capelin growth. *ICES Marine Science Symposium* **195**, pp. 278–290.

Skogen, M., Søiland, H., 1998. A user guide to NORWECOM v2.0, The Norwegian Ecological Model System. Fisken og Havet, 18, Institute of Marine Research, Norway, p. 42.

Stenseth, N.C., Mysterud, A., Ottersen, G., Hurrell, J.W., Chan, K.-S. and Lima, M., 2002. Ecological Effects of Climate Fluctuations. *Science* **297**, pp. 1292–1296.

Sætre, R., Ljøen, R., 1971. The Norwegian Coastal Current. In: Anon (Ed.), Proceedings of the First International Conference on Port and Ocean Engineering under Arctic Conditions, Vol. II. Technical University of Norway, Trondheim, p. 20.

Sætre, R., Aure, J. and Ljøen, R., 1998. Wind effects on the lateral extension of the Norwegian Coastal Water. *Continental Shelf Research* **8**, pp. 239–253.

Woodgate, R.A., Aagaard, K., Muench, R.D., Gunn, J., Björk, G., Rudels, B., Roach, A.T. and Schauer, U., 2001. The Arctic Ocean Boundary Current Along the Eurasian slope and the adjacent Lomonosov Ridge: water mass properties transports and transformations from moored current meters. *Deep-Sea Research I* **48**, pp. 1757–1792.

Appendix A. Mesoscale activity

The presence of mesoscale eddies can seriously alias the result when estimating volume fluxes from moored current meters. Although eddies in the area are limited in both time and space (Loeng and Sætre, 2001), eddies with periods of about 1 month have been observed (Ingvaldsen et al., 2002). The presence of eddies should show up as large differences between transport series calculated with different spatial resolution. To investigate the reliability of our transport series, transports for the period of September 2000–August 2001 were calculated based on 7 moorings and based on 5 moorings after replacing

mooring Nos. 2b and 3b with the mean of the adjacent moorings (see Fig. 2). The resolution in the middle part was 25 and 50 km, respectively. Note that prior to the calculations, the velocity data were filtered with a 14-days lowpass filter. The results show surprisingly small differences (Fig. 12). Although there are indications that mooring No. 2b at times captured a weak return flow or an area of stagnant water which the nearby moorings fail to capture (not shown), a doubling of the resolution does not generally alter the transport values. The largest differences appear during periods of local maximum and minimum transport when the higher resolution sometimes gives higher transports and sometimes lower. The mean of the difference between the two transport series is 0.0, and the error of the mean is ±0.1 Sv. The transport fluctuations are somewhat sensitive to the increased resolution, but the correlation coefficient is 0.93, i.e. 5 moorings deployed with a mutual distance of 50 km capture 86% of the variability. The relatively good accordance between these two transports series indicates that the influence of mesoscale eddies probably is small when considering fortnightly or longer time scales, i.e. they will not seriously affect the transport series.

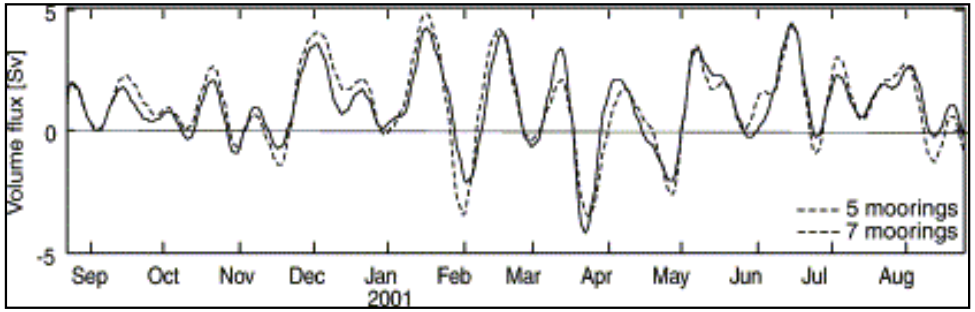

Fig. 12. Transport of AW across the section as estimated from the current measurements using 5 and 7 moorings. Positive transport is into the Barents Sea (i.e. eastward).

Appendix B. Error estimates on the mean transports

The transport estimates are subject to errors in the measured velocities, and of the calculation method. The errors in the current measurements are small due to calibration and a large number of individual samples.

The uncertainties in the calculation methods are partly due to the variability in time. The presence of mesoscale eddies can create large errors in the transports; therefore, fortnightly means were calculated before the transports were estimated (Appendix A). To quantify the error associated with fortnightly means due to the eddy noise, the standard error of the mean (*S.E.*) was calculated. This is given by $S.E. = S(x,z)/\sqrt{n}$ where $S(x,z)$ is the empirical standard deviation at a given instrument and n is the number of degrees of freedom (or number of independent time steps). Individual samples are not

independent, and *n* was found for each instrument by the autocorrelation function. *S.E.* was calculated for each instrument, and weighted by the area represented by the instruments to give an error estimate for the velocity means.

Errors also arise due to the extrapolation of each current meter to represent boxes with uniform velocity. Assuming a monotonic structure between the instruments, the error will be small when two adjacent moorings sample almost the same velocity and large when the adjacent moorings have a large velocity difference. Using the same methods as Fachbach et al. (2001) for current measurements in the Fram Strait, the error was expressed by the mean of the velocity difference between the adjacent points. The error of the velocity difference mean was then found as for the error of the velocity means. It turned out that this error was about the same size as the error of the velocity means.

The largest errors occur if the velocity structure between adjacent moorings is not monotonic, but as shown in Appendix A the mean of the difference between the transport series calculated for five and seven moorings is 0.0, and the error of the mean is ±0.1 Sv. This is much less than the errors obtained by the velocity difference between the adjacent moorings. The presented errors, which are a combination of the errors obtained from the mean velocities and the box method, may therefore be considered worst-case error estimates for the transports. Note that the error estimates hereafter presented are errors for the mean; they should not be interpreted as an error for the actual transport at a given time.

---

[1] This should be adequate as temperature is the characteristic parameter separating AW from the outflowing water masses in the north. Salinity is the key for separating the AW from the Coastal Water, but as the Coastal Water occurs mostly in the upper 50 m in the area of the moorings, it will not seriously affect our estimates.